Philosophical Magazine
Vol. 88, Nos. 30–32, 21 October–11 November 2008, 3527–3548

Downloaded By: [Oak Ridge National Laboratory] At: 20:54 4 September 2009

On the elastic boundary value problem of dislocations in bounded crystals

J. Deng[a], A. El-Azab[ab]* and B.C. Larson[c]

[a]*Mechanical Engineering Department, Florida State University, Tallahassee, US;* [b]*School of Computational Science, Florida State University, Tallahassee, US;* [c]*Materials Science and Technology Division, Oak Ridge National Laboratory, Oak Ridge, US*

(*Received 31 December 2007; final version received 8 October 2008*)

A new formulation of the elastic boundary value problem of dislocations in bounded crystals is developed. This formulation is based on the ansatz that the stress field of dislocations in bounded domains can be constructed as the sum of a contribution corresponding to the classical infinite-domain solution plus a correction that is determined here from a mathematically well posed problem. The formulation of the elastic boundary value problem given here ensures that the equilibrium of the overall stress field is rigorously satisfied, specifically when dislocations intersect the boundary. The implications of this new formalism for dislocation dynamics simulation are discussed for the cases of bounded crystals and crystal volumes representative of uniformly loaded infinite crystals. An approximate computational solution of the elastic boundary value problem is presented based on the concept of virtual dislocations and the use of a non-singular form of the infinite-domain solution of the dislocation stress field. This computational solution addresses the issues of singularity and global equilibrium of the boundary traction associated with the corrective field. Sample results are presented for the internal stress in bounded crystals containing 3D dislocation configurations produced using the dislocation dynamics simulation method. The results illustrate the statistical character of the internal elastic field.

Keywords: defects in solids; deformation mechanisms; dislocation dynamics; dislocation mechanics; dislocation theory

1. Introduction

Complex dislocation structures emerge during plastic deformation of crystals. The evolution of such structures is strongly influenced by various aspects of the physical behavior of dislocations, one of which is their long-range elastic interactions. These interactions are governed by the internal crystal stress generated by the dislocations themselves, which is obtained by solving the elastic boundary value problem of the crystal domain containing the dislocation configuration under consideration. The solution of this problem is an important part of the method of dislocation dynamics simulation [1–4]. Indeed, the majority of the computational effort in this method is associated with the solution of the elastic boundary value problem of dislocations and the computation of

*Corresponding author. Email: anter@eng.fsu.edu

ISSN 1478–6435 print/ISSN 1478–6443 online
© 2008 Taylor & Francis
DOI: 10.1080/14786430802558544
http://www.informaworld.com

their mutual long-range interactions [1–6]. In setting up this boundary value problem, two situations have been commonly treated in the literature. The first is that of a bounded crystal, and the second is one in which the crystal volume containing the dislocation system under consideration is a representative volume element (RVE) whose average response is the same as that of a large, infinitely extended crystal. The boundary conditions for these two problems have been developed previously by one of the authors [7] who also performed a limited numerical implementation for the stress field of dislocation loops contained in a rectangular 3D crystal region [8].

The formulation presented in [7] for the elastic boundary value problem of dislocations in the two situations mentioned above is based on the postulate that the stress $\boldsymbol{\sigma}$ of an arbitrary dislocation configuration contained in a finite crystal volume Ω representing an RVE or in a bounded crystal is expressed as the sum of two contributions. The first is the infinite-domain stress of the dislocation configuration contained in Ω, which is denoted here by $\boldsymbol{\sigma}^{\infty}$, and the second is a corrective field $\tilde{\boldsymbol{\sigma}}$; that is

$$\boldsymbol{\sigma}(\mathbf{x}) = \boldsymbol{\sigma}^{\infty}(\mathbf{x}) + \tilde{\boldsymbol{\sigma}}(\mathbf{x}), \tag{1}$$

where $\mathbf{x}$ denotes the position vector in Ω. The stress $\tilde{\boldsymbol{\sigma}}$ satisfies the traction boundary condition

$$\tilde{\boldsymbol{\sigma}}(\mathbf{x})\mathbf{n}(\mathbf{x}) = \tilde{\mathbf{t}}(\mathbf{x}) = -\boldsymbol{\sigma}^{\infty}(\mathbf{x})\mathbf{n}(\mathbf{x}), \tag{2}$$

in which $\mathbf{n}$ is the outward unit normal to the boundary $\partial\Omega$. Equation (2) implies the well-known result that the overall dislocation stress field $\boldsymbol{\sigma}$ satisfies a traction-free boundary condition. We remark here that while the decomposition (1) of the stress field (and actually all elastic fields) is valid when Ω is an RVE or a bounded crystal, the field $\tilde{\boldsymbol{\sigma}}$ and the associated displacement and strain fields can be called image fields only in the case of bounded crystals. In the case of a RVE, however, such a contribution represents the stress induced inside Ω by dislocations in the rest of the extended crystal. In [7] an argument about statistical homogeneity of elastic fields in the infinite crystal has been followed to show that the $\tilde{\boldsymbol{\sigma}}$ is equal to the image stress of dislocations if the RVE is viewed as a bounded crystal. A recent implementation in the ParaDiS dislocation dynamics simulation model [3] satisfies the requirement of statistical homogeneity of fields in an infinite crystal by applying periodic boundary conditions to the RVE. In this case the $\tilde{\boldsymbol{\sigma}}$ field is computed by summing up the contributions due to periodic replicas of the dislocation configuration.

The formulation and solution of the elastic boundary value problem of dislocations has been pursued by a number of authors in the case of bounded crystals. Van der Giessen and Needleman [5] set up a formalism of this problem based on the principle of superposition in linear elasticity, which was implemented later for 3D problems by Weygand et al. [6] who addressed two issues. The first has to do with the fact that when dislocations end on the boundary $\partial\Omega$, the residual boundary traction $\tilde{\mathbf{t}}$ (computed using the classical line-integral form for dislocation stress) is not self-balanced because the line-integral form of stress field does not satisfy equilibrium in this case. In other words, the global equilibrium conditions,

$$\int_{\partial\Omega} \tilde{\mathbf{t}}(\mathbf{x})\mathrm{d}A = 0 \quad \text{and} \quad \int_{\partial\Omega} \tilde{\mathbf{t}}(\mathbf{x}) \times (\mathbf{x} - \mathbf{x}_{\circ})\mathrm{d}A = \mathbf{0}, \tag{3}$$

Downloaded By: [Oak Ridge National Laboratory] At: 20:54 4 September 2009

are violated (dA is a differential surface element of the boundary $\partial\Omega$ and $\mathbf{x}_\circ$ is some point in Ω). When the dislocation network is closed, and none of the dislocations is ending on the surface, the above integrals are identically zero and the residual traction $\tilde{\mathbf{t}}$ defines a well-posed elastic boundary value problem for the image stress $\tilde{\boldsymbol{\sigma}}$. The issue of self-balance of the image traction has been dealt with by keeping the dislocation network closed using virtual dislocation segments outside Ω and using the field of these virtual segments in computing the residual traction of dislocations on the boundary. The second issue addressed in [6] is that the classical linear elasticity solution of dislocation fields is singular along the dislocation lines. This posed a numerical difficulty in treating the residual traction on the boundary in a finite-element formulation of the image field problem, which was dealt with by using higher quadrature order.

Tang et al. [9] presented a boundary value problem formulation for the image field, in which the singular part of the traction of the image field is analytically considered, while the rest of the image field is computed by applying a non-singular traction term using the finite element method (FEM). The famous Yoffe solution [10] for the elastic fields of straight dislocations in a half space, see also [11], was used by Tang et al. to find the solution corresponding to the singular part of the residual traction. In Tang's work, however, the global equilibrium requirement for the residual traction, an essential condition of well posedness of the boundary value problem, was not checked. Other attempts to solve this problem have been made. For example, a boundary element method (BEM) was developed recently by El-Awady et al. [12] to compute the image stress field of dislocations for use in dislocation dynamics simulation of micropillar deformation. Khraishi et al. [13] used surface distributions of prismatic dislocation loops to satisfy the traction free boundary condition on the surfaces of a rectangular dislocation dynamics simulation volume. Weinberger and Cai [14] developed semi-analytical solutions for the image field in cylindrical micropillars.

In all of these works, the stress field of dislocations in bounded domains was constructed as the sum of the classical line-integral form for stress, which is given later in this paper, plus an image correction. In formulating the boundary value problem for the image field, however, authors focused only on the fact that the overall stress field is traction free, which defines the traction boundary condition for the image field. When dislocations end on the surface, the line-integral form does not yield a divergence-free stress field. This fact, which has been overlooked so far, makes it necessary to include a distributed body force in the image-field boundary value problem to ensure that the overall stress field is divergence free.

Lemarchand et al. [15,16] approached the problem of finding the stress field in a crystal with a dynamic dislocation configuration by using the FEM method to solve a crystal plasticity problem in which the plastic strain is found from the dislocation motion. In this method, stress equilibrium is handled properly, but the localization of plastic strain on slip planes posed some numerical issues that were resolved by defining an appropriate volume averaging scheme for the induced plastic strain. The approach of Lemarchand et al. is equivalent to the eigenstrain formalism of plastic deformation [17]. Finally, an approximation of the boundary problem of dislocations by Schwarz [18] should be mentioned. In this approximation, an image construction is used in which part of the dislocation intersecting the boundary is reflected across the boundary and the effect of the image is included in evolving of the interior near-boundary segments in dislocation dynamics simulation.

Downloaded By: [Oak Ridge National Laboratory] At: 20:54 4 September 2009

The present paper has three objectives. The first objective is to use the eigenstrain formalism of the boundary value problem of dislocations in bounded crystals to provide a theoretical justification for constructing the solution in terms of the infinite-domain solution plus image correction. For this purpose, we follow the formulation by Kinoshita and Mura [19] of the eigenstrain problem in finite elastic body. The second objective is to provide the correct statement of the image-field boundary value problem for an arbitrary dislocation configuration in bounded crystals and to discuss the implications of this statement in the context of the dislocations dynamics simulation. In particular, we suggest a formulation of dislocation dynamics with a scheme for long-range stress calculation that is both simple and accurate. The third objective of this paper is to present an approximate solution of the image stress problem in the spirit of the virtual dislocation technique given by Weygand et al. [6]. The motivation for pursuing this approximate solution is to test the effectiveness of using the non-singular infinite domain expression of the dislocation stress field developed by Cai et al. [20] in solving the image field problem using the FEM method. As shown later, the use of this non-singular stress expression makes it a straightforward task to solve the problem. The results show that the stress field in a crystal with high dislocation density exhibits strong spatial fluctuations. Such fluctuations are relevant to sub-micrometer resolution 3D X-ray microscopy measurements of elastic fields in deformed crystals [21,22].

Downloaded By: [Oak Ridge National Laboratory] At: 20:54 4 September 2009

2. Eigenstrain formalism of the boundary value problem

The eigenstrain theory offers a powerful approach to solving the class of problems of internal elastic fields of defects in materials [17]. In this theory, material defects are modeled using equivalent incompatible stress-free strain distributions called the eigenstrains. The eigenstrain problem is stated as follows: find the displacement, elastic strain and stress fields in a domain Ω, due to an arbitrary eigenstrain distribution $\boldsymbol{\varepsilon}^*(\mathbf{x})$. In the absence of body forces, the equations governing the eigenstrain problem are

$$\begin{aligned} \text{stress equilibrium:} \quad & \operatorname{div}\boldsymbol{\sigma} = \mathbf{0}, \\ \text{stress-strain law:} \quad & \boldsymbol{\sigma} = \mathbf{c} : \boldsymbol{\varepsilon}^{\mathrm{e}} = \mathbf{c} : (\boldsymbol{\varepsilon} - \boldsymbol{\varepsilon}^*), \\ \text{strain-displacement relationship:} \quad & \boldsymbol{\varepsilon} = \operatorname{Sym}\operatorname{grad}\mathbf{u}. \end{aligned} \tag{4}$$

In these equations, $\boldsymbol{\sigma}$ is the internal stress, $\mathbf{c}$ the elasticity tensor of the medium, $\boldsymbol{\varepsilon}^{\mathrm{e}}$ the elastic strain, $\boldsymbol{\varepsilon}$ the total strain, $\mathbf{u}$ the displacement field, and $\operatorname{Sym}\operatorname{grad}\mathbf{u}$ denotes the symmetric part of the displacement gradient. The boundary conditions depend on the specific situation. In the case of an infinite domain, the eigenstrain distribution must vanish faster than $|\mathbf{x}|^{-1}$ as $|\mathbf{x}| \to \infty$ for the problem to admit a solution. In the case of dislocations, the eigenstrain is prescribed by the symmetric part of the plastic distortion tensor resulting from the introduction of dislocations in the crystal. Here, we consider a set of dislocation lines each of which bounds a slipped area on a particular crystallographic slip plane. In this case, the total plastic distortion tensor $\boldsymbol{\beta}^{\mathrm{p}}$ is given by

$$\boldsymbol{\beta}^{\mathrm{p}} = -\sum_{\alpha} \boldsymbol{\delta}(S^{\alpha}) \otimes \mathbf{b}^{\alpha}, \tag{5}$$

in which $\mathbf{b}^{\alpha}$ is the Burgers (slip) vector corresponding to the αth slip area S^{α}, $\boldsymbol{\delta}(S^{\alpha})$ is the (vector) dirac-delta distribution defined over S^{α}, and $\boldsymbol{\delta}(S^{\alpha}) \otimes \mathbf{b}^{\alpha}$ denotes the tensor product

of the two vectors. It is assumed here that each of the slip areas S^α is bounded by a dislocation line L^α. In the case of an infinite domain, the set of dislocation lines can be in the form of isolated loops, a closed network, or a mix of both. According to Mura [17] and de Wit [23], the solution of this problem for a single dislocation loop is expressed analytically in the form of a line integral along the loop with a kernel involving the infinite-domain elastic Green function $\mathbf{G}(\mathbf{x}-\mathbf{x}')$. Generalizing the results to a set of loops, the corresponding displacement field $\mathbf{u}$, the elastic part of the displacement gradient $\boldsymbol{\beta}^{\mathrm{e}}_{mn}$, which is known as the elastic distortion, and the stress field can be written in the form

$$
\begin{aligned}
u_m(\mathbf{x}) &= \sum_\alpha \int_{S^\alpha} c_{ijkl} G_{jm,i}(\mathbf{x}-\mathbf{x}') b^\alpha_l m^\alpha_k(\mathbf{x}') \mathrm{d}A', \\
\boldsymbol{\beta}^{\mathrm{e}}_{mn}(\mathbf{x}) &= u_{m,n}(\mathbf{x}) - \boldsymbol{\beta}^{\mathrm{p}}_{mn}(\mathbf{x}) = \sum_\alpha \oint_{L^\alpha} \epsilon_{pmk} c_{ijkl} G_{jn,i}(\mathbf{x}-\mathbf{x}') b^\alpha_l \xi^\alpha_p(\mathbf{x}') \mathrm{d}\ell', \\
\sigma_{ij}(\mathbf{x}) &= c_{ijmn}\varepsilon^{\mathrm{e}}_{mn} = c_{ijmn}\beta^{\mathrm{e}}_{mn} = \sum_\alpha \oint_{L^\alpha} \epsilon_{pmk} c_{ijmn} c_{ijkl} G_{jn,i}(\mathbf{x}-\mathbf{x}') b^\alpha_l \xi^\alpha_p(\mathbf{x}') \mathrm{d}\ell',
\end{aligned}
\tag{6}
$$

where ϵ_{pmk} denotes the permutation tensor, $\boldsymbol{\xi}$ the unit tangent along the dislocation line, $\mathbf{m}^\alpha$ the unit normal to S^α, and $\boldsymbol{\varepsilon}^{\mathrm{e}} = \mathrm{Sym}\,\boldsymbol{\beta}^{\mathrm{e}}$. We note that the equality $\mathbf{c}:\varepsilon^{\mathrm{e}} = \mathbf{c}:\beta^{\mathrm{e}}$ follows from the symmetry property $c_{ijmn} = c_{ijnm}$ of the elasticity tensor $\mathbf{c}$.

In the case of a bounded crystal, the formulation of the eigenstrain problem must also include the specification of the traction and/or the displacement boundary condition on $\partial\Omega$. Here, we consider an eigenstrain problem with a traction-free boundary condition. We note, however, that it is possible to superpose solutions corresponding to a prescribed traction and/or displacement condition on $\partial\Omega$, once the eigenstrain part of the problem is solved. In the case of a bounded domain, the eigenstrain problem is again described by Equations (4), but it is now subject to the boundary condition $\boldsymbol{\sigma}(\mathbf{x})\mathbf{n}(\mathbf{x}) = \mathbf{0}$ on $\partial\Omega$, which can be handled numerically, such as by FEM, as was done by Lemarchand et al. [15,16], or analytically. Analytical solutions of this type of problem usually involve volume integrals of some kernel times the plastic distortion $\boldsymbol{\beta}^{\mathrm{p}}$. Indeed, the integral representation of the solution of the eigenstrain problem in bounded domains involves the so-called Neumann tensor as a kernel [19]. This tensor is the bounded-domain counterpart of the infinite-domain elastic Green function $\mathbf{G}(\mathbf{x}-\mathbf{x}')$.

Kinoshita and Mura [19] and Mura [24] developed an integral representation of the solution of the eigenstrain problem for dislocation loops. Mura's results [24] for the displacement, elastic distortion and stress fields were expressed in terms of the corresponding plastic distortion as follows:

$$
\begin{aligned}
u_j(\mathbf{x}) &= \int_\Omega c_{lmpq} N_{jl,m'}(\mathbf{x},\mathbf{x}') \beta^{\mathrm{p}}_{pq}(\mathbf{x}') \mathrm{d}\Omega', \\
\beta^{\mathrm{e}}_{jk}(\mathbf{x}) &= \int_\Omega c_{lmpq} N_{jl,m'k}(\mathbf{x},\mathbf{x}') \beta^{\mathrm{p}}_{pq}(\mathbf{x}') \mathrm{d}\Omega' - \beta^{\mathrm{p}}_{jk}, \\
\sigma_{hi}(\mathbf{x}) &= c_{hijk} \int_\Omega c_{lmpq} N_{jl,m'k}(\mathbf{x},\mathbf{x}') \beta^{\mathrm{p}}_{pq}(\mathbf{x}') \mathrm{d}\Omega' - c_{hijk}\beta^{\mathrm{p}}_{jk},
\end{aligned}
\tag{7}
$$

in which the tensor N_{ij} is the elastic Neumann tensor and the comma notation involving a primed index indicates differentiation with respect to the primed coordinate. We keep in mind that in the case of a discrete dislocation distribution the tensor β^{p} is given by

Downloaded By: [Oak Ridge National Laboratory] At: 20:54 4 September 2009

Equation (5), and thus the volume integrals in Equation (7) reduce to integrals over the slipped areas. As shown by Mura [24], however, such surface integrals further reduce to line integrals along the dislocation lines in the expressions for stress and elastic strain. The Neumann tensor N_{ij} appearing in the integral solution form (7) is given by

$$N_{jl}(\mathbf{x}, \mathbf{x}') = G_{jl}(\mathbf{x} - \mathbf{x}') + H_{jl}(\mathbf{x}, \mathbf{x}'), \tag{8}$$

where $G_{jl}(\mathbf{x} - \mathbf{x}')$ is the infinite-domain elastic Green function and the tensor $H_{jl}(\mathbf{x}, \mathbf{x}')$ is the solution of the differential equation

$$c_{hijk} H_{jl,ki}(\mathbf{x}, \mathbf{x}') = w_{hl}(\mathbf{x}, \mathbf{x}'), \tag{9}$$

subject to the boundary condition

$$c_{hijk} n_i(\mathbf{x}) H_{jl,k}(\mathbf{x}, \mathbf{x}') = -c_{hijk} n_i(\mathbf{x}) G_{jl,k}(\mathbf{x} - \mathbf{x}'). \tag{10}$$

In the above, $\mathbf{n}$ is the unit outward normal to $\partial\Omega$, as previously specified, and the tensor-valued function w_{hl} is given by

$$w_{hl}(\mathbf{x}, \mathbf{x}') = |\Omega|^{-1} \delta_{hl} + \epsilon_{hij} \Lambda^{-1}_{jm} \epsilon_{mlk} (\gamma_i - x_i)(\gamma_k - x'_k), \tag{11}$$

with $|\Omega|$ being the volume of Ω and Λ^{-1}_{jm} the inverse of the tensor Λ_{jm} defined by

$$\Lambda_{jm} = \delta_{jm} \lambda_{ii} - \lambda_{jm}. \tag{12}$$

In the above formulae, the tensor λ_{jm} and the vector γ_i are defined by

$$\lambda_{jm} = \int_\Omega (\gamma_j - x_j)(\gamma_m - x_m) \mathrm{d}\Omega \quad \text{and} \quad \gamma_i = |\Omega|^{-1} \int_\Omega x_i \mathrm{d}\Omega. \tag{13}$$

A few remarks are in order regarding the Kinoshita-Mura solution of the bounded-domain eigenstrain problem. First, we note that (as asserted by the additive decomposition of the Neumann tensor) the solution of this problem can be split into two parts, one part corresponding to the infinite-domain problem and the other being the image field. Next, when a bounded domain is free of external traction or displacement constraints, the issue of global equilibrium of the domain becomes important. Indeed, the overall force and moment balance was enforced in fixing the solution of the bounded-domain eigenstrain problem in [19]. Furthermore, although splitting the overall solution into an infinite-domain contribution plus an image correction supports the ansatz of additive decomposition of the solution (1), this decomposition cannot be classified as a superposition in the strict sense of the term in the theory of linear elasticity. In linear elasticity, superposition rather implies that more than one solution, each of which corresponds to a well-posed boundary value problem, are added together to obtain the solution corresponding to the sum of the boundary conditions and/or sources associated with the individual problems. In the case of dislocations in a bounded crystals, the infinite-domain contribution may or may not constitute a solution of a well-posed problem, depending on whether the dislocation configuration is closed inside the boundary or open with lines ending on the boundary. Finally, we emphasize that the solution of the subsidiary boundary value problem given by Equations (9) through (11) is still required to complete the eigenstrain problem solution. In the case of dislocations, this subsidiary boundary value problem is recast in the form of a problem of finding a fourth-order tensor field [24].

Downloaded By: [Oak Ridge National Laboratory] At: 20:54 4 September 2009

Downloaded By: [Oak Ridge National Laboratory] At: 20:54 4 September 2009

3. A new statement of the boundary value problem

In dislocation dynamics simulation models, the infinite-domain stress expression for dislocation segments (of finite or differential length) provides a basis for computing the long-range interactions of dislocations. As far as bounded crystal volumes are concerned, the Kinoshita-Mura line integral form for the elastic field of dislocations [24] can also be cast as a sum of contributions by dislocation segments. However, the implementation of the Kinoshita-Mura formalism requires the solution of an additional boundary value problem to completely fix the Neumann tensor field. On the other hand, compared with the Kinoshita-Mura formalism, the decomposition ansatz discussed earlier for the overall stress field of dislocations, see Equation (1), is more attractive because methods such as FEM or BEM can be used to solve the image field problem systematically. Before pursuing this approach, it is important to fix the statement of the image field boundary value problem.

As stated earlier, previous attempts to fix this problem focused on satisfying the traction-free boundary condition but overlooked the development of a correct local form for stress equilibrium. That is, the problem was set up based on the assumption that the image field is completely fixed by the boundary condition that the overall stress field is traction free. Of course this assumption is justified if the dislocation configuration is fully contained within the finite domain Ω, with no dislocations ending on its boundary. However, when dislocations end on the boundary a different treatment is required and a new statement of the boundary value problem is needed for the image field of dislocations in bounded domains.

The starting point for studying the stress equilibrium for dislocations in a bounded domain with a traction free boundary is to enforce the following two conditions on the overall stress field,

$$\begin{aligned} &\operatorname{div}\boldsymbol{\sigma}(\mathbf{x}) = \operatorname{div}(\boldsymbol{\sigma}^{\infty}(\mathbf{x}) + \tilde{\boldsymbol{\sigma}}(\mathbf{x})) = \mathbf{0}, \quad \mathbf{x} \in \Omega, \\ &(\boldsymbol{\sigma}^{\infty} + \tilde{\boldsymbol{\sigma}})\mathbf{n}(\mathbf{x}) = \mathbf{0}, \qquad \mathbf{x} \in \partial\Omega, \end{aligned} \tag{14}$$

where $\boldsymbol{\sigma}^{\infty}$ is the stress field of the dislocation configuration computed using the famous line-integral form used in infinite-domain problems, see for example Equation (17), and $\tilde{\boldsymbol{\sigma}}$ is the image stress field. The former contribution may of course be cast as the sum of contributions by individual segments contained in Ω. It is important to note here that the decomposition of the total stress field into two components can be arbitrary and that specifying one of these components to be the stress field of the dislocation configuration in an infinite medium is a matter of convenience in the present case. Making use of the fact that the Kinoshita-Mura solution discussed above shows that taking the infinite-domain stress of dislocations as a part of the overall stress field is a natural choice, the conditions in Equation (14) lead to the following statement of the elastic boundary value problem for the image stress field of dislocations in a bounded domain:

$$\begin{aligned} \text{stress equilibrium:} \quad & \operatorname{div}\tilde{\boldsymbol{\sigma}}(\mathbf{x}) + \tilde{\mathbf{f}}(\mathbf{x}) = \mathbf{0}, \quad \tilde{\mathbf{f}}(\mathbf{x}) = \operatorname{div}\boldsymbol{\sigma}^{\infty}(\mathbf{x}), \quad \mathbf{x} \in \Omega, \\ \text{traction boundary condition:} \quad & \tilde{\boldsymbol{\sigma}}\mathbf{n}(\mathbf{x}) = \tilde{\mathbf{t}}(\mathbf{x}), \quad \tilde{\mathbf{t}}(\mathbf{x}) = -\boldsymbol{\sigma}^{\infty}(\mathbf{x})\mathbf{n}(\mathbf{x}), \quad \mathbf{x} \in \partial\Omega, \\ \text{stress-strain law:} \quad & \tilde{\boldsymbol{\sigma}} = \mathbf{c} : \operatorname{Sym}\operatorname{grad}\tilde{\mathbf{u}}. \end{aligned} \tag{15}$$

Here $\tilde{\mathbf{u}}$ is the image displacement field. It is clear that, in addition to the traction boundary condition specified by $\tilde{\mathbf{t}}$ on $\partial\Omega$, which is the inverse of the residual traction left by the

infinite-domain solution, the image field is in general not divergence free. Rather, its divergence is equal to a distributed body force completely fixed by the divergence of the stress field $\boldsymbol{\sigma}^{\infty}$ of the dislocation configuration, which is computed as if the dislocations were contained in an infinite domain. We remark here that the body force $\tilde{\mathbf{f}} = \operatorname{div} \boldsymbol{\sigma}^{\infty}(\mathbf{x})$ vanishes identically if the dislocation configuration in Ω is fully closed. We remark further that additional external traction or displacement conditions can be added to the above statement of the boundary value problem by the usual superposition principle of linear elasticity.

We note that the overall stress field of dislocations in a bounded domain Ω can be fixed completely by solving the boundary value problem given in Equation (15) for the image stress, and adding to this solution the infinite-domain stress contribution by the dislocation segments contained in Ω. An implementation of this approach is in progress. We anticipate that the use of FEM to solve the (elastic) image field problem (15) will be easier than the approach of Lemarchand et al. [15,16]. This is because the FEM solution of the elastic image field problem is much less computationally intensive than solving the combined crystal-plasticity/dislocation-dynamics problem. Moreover, the scheme developed here will be simpler than dealing with the subsidiary boundary value problem required to fix the Neumann tensor field in the Kinoshita-Mura formulation.

The following global equilibrium conditions follow from the statement of the boundary value problem given in Equation (15) above:

$$\begin{aligned} \text{null force resultant:} \quad & \int_{\partial\Omega} \tilde{\mathbf{t}}(\mathbf{x}) \mathrm{d}A + \int_{\Omega} \tilde{\mathbf{f}}(\mathbf{x}) \mathrm{d}\Omega = \mathbf{0}, \\ \text{null moment resultant:} \quad & \int_{\partial\Omega} \tilde{\mathbf{t}}(\mathbf{x}) \times (\mathbf{x} - \mathbf{x}_{\circ}) \mathrm{d}A + \int_{\Omega} \tilde{\mathbf{f}}(\mathbf{x}) \times (\mathbf{x} - \mathbf{x}_{\circ}) \mathrm{d}\Omega = \mathbf{0}. \end{aligned} \tag{16}$$

As will be shown below, these conditions are important for testing the accuracy of the finite element solution of the image field boundary value problem. For this purpose, the first of these conditions is sufficient as the second follows from the first and the symmetry of the stress tensor.

4. Implications for the method of dislocation dynamics simulation

In dislocation dynamics simulations, the crystal volume under consideration is always finite. Depending on the imposed boundary conditions, this volume can represent a bounded crystal or a RVE whose (average) response is equivalent to the response of a uniformly loaded infinite crystal. The question of which boundary conditions apply to the simulation volume in the two cases has been addressed previously by El-Azab [7], where two types of boundary conditions were formulated, the elastic boundary conditions and the dislocation flux boundary condition. With regard to the elastic boundary condition, it was shown for the case of a bounded crystal that the total stress field in the crystal consists of the infinite-domain stress field of dislocations plus an image field determined such that the crystal surface remains traction free. In the case of an RVE, on the other hand, the requirement that the volume average of the RVE response be equal to the average response of the infinite crystal leads to the conditions that the average of the dislocation stress field over the RVE must vanish. This condition implies that the stress contribution within the

Downloaded By: [Oak Ridge National Laboratory] At: 20:54 4 September 2009

RVE by dislocations from outside the RVE is the same as the image field of dislocations contained within the RVE itself.

The important inference to draw from the above result is that the bounded crystal and the RVE situations are basically the same when it comes to internal stress computation. However, for the case of a bounded crystal, as pointed out in the introduction, only the method by Lemarchand and coworkers [15] yields an accurate solution, albeit at the cost of solving a relatively complex plasticity problem by the FEM method. For the case of an RVE, on the other hand, the available simulation models employ periodic boundary conditions to enforce statistical homogeneity; see for example the ParaDiS model [3]. This periodicity entails a significant complexity in computing the image field. An early proposal for computing the image field in the context of periodic boundary conditions was to use the minimum image convention and a pre-tabulation and interpolation scheme of long range stress [25]. Basically, in [25] the stress field of differential dislocation segments was pre-tabulated with both the source and field points on a regular grid, which was then interpolated for use during the actual field computation. Unfortunately, the minimum image convention procedure does not capture the long range interactions well because these interactions are cut off beyond one box size. Consideration of more complete periodic sums and their conditional convergence in the case of dislocation dynamics has been addressed in [26]. In actual implementation, however, the sum is taken over a large number of images.

Based on the above observations, it is clear that the problem of stress computation in dislocation dynamics simulation requires further improvement. The formulation of this problem given in the previous section provides a powerful alternative in this regard that is both simple and exact, since it satisfies the stress equilibrium rigorously for both the bounded crystal and RVE situations. For the RVE case in particular, this will give a self-consistent representation of the elastic interactions between the dislocations in the central simulation volume and in the rest of the infinite crystal, without making any assumptions (e.g. periodicity) about the dislocation structure outside the simulation volume. Compared with periodic boundary conditions, this is indeed a remarkable development.

5. Approximate solution

The solution of the exact boundary value problem (15) is in progress. In this section, however, an approximate solution based on the virtual dislocation concept [6] is pursued to gain insight into the convergence characteristics of the solution and to provide a means for comparison with the solution of the exact boundary value problem. The implementation of the virtual dislocation solution here differs from that reported in [6] in two respects. First, we ensure the equilibrium of the reversed traction, in the sense of Equation (3), by extending the segments touching the surface of the domain of solution to infinity. Second, to compute the traction boundary condition for the image field, we use the non-singular stress solution developed in [20] for the field $\boldsymbol{\sigma}^{\infty}$. We note here that the extension to infinity of the segments touching the surface can be done arbitrarily, which renders the contribution to $\tilde{\mathbf{t}}$ by the (virtual) dislocations outside Ω dependent on how the configuration of these dislocations is constructed. This does not pose a serious issue, though, because the error associated with the construction of the virtual dislocation configuration is much smaller than the error arising due to the violation of equilibrium if

Downloaded By: [Oak Ridge National Laboratory] At: 20:54 4 September 2009

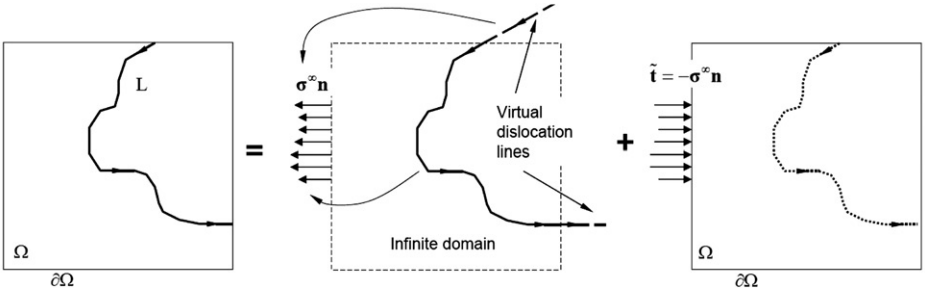

Figure 1. Illustration of the superposition principle with virtual dislocations.

such dislocations were completely ignored. With this argument justifying the use of virtual dislocations to approximate the image field, we will test the effectiveness of combining the finite element method and the non-singular infinite domain solution of dislocation segments for computing the image stress field.

The superposition principle used with the virtual dislocation method is illustrated in Figure 1. Because the actual dislocation structure is augmented by semi-infinite segments, the infinite domain solution of the extended dislocation system is divergence-free. Consequently, the image field is also divergence free and satisfies the boundary condition $\tilde{\boldsymbol{\sigma}}\mathbf{n} = \tilde{\mathbf{t}} = -\boldsymbol{\sigma}^{\infty}\mathbf{n}$ on the boundary $\partial\Omega$. This problem is solved here using FEM, where $\boldsymbol{\sigma}^{\infty}$ has contributions from both the actual dislocation configuration within the solution domain and the virtual dislocation extensions outside this domain. The non-singular form of $\boldsymbol{\sigma}^{\infty}$ developed in [20] is used in the current implementation, which is denoted here by $\boldsymbol{\sigma}^{\mathrm{ns},\infty}$. For a dislocation loop L in an infinite isotropic medium, this stress field is expressed in the form

$$\sigma_{\alpha\beta}^{\mathrm{ns},\infty}(\mathbf{x}) = \frac{\mu}{8\pi}\oint_L \partial_i\partial_p\partial_p R_a\Big[b_m\epsilon_{im\alpha}\,\mathrm{d}x'_\beta + b_m\epsilon_{im\beta}R_a\,\mathrm{d}x'_\alpha\Big] + \frac{\mu}{4\pi(1-\nu)}\oint_L b_m\epsilon_{imk}\big[\partial_i\partial_\alpha\partial_\beta R_a - \delta_{\alpha\beta}\partial_i\partial_p\partial_p R_a\big]\mathrm{d}x'_k, \tag{17}$$

where $\partial_i \equiv \partial/\partial x_i$, $R_a = \sqrt{R^2 + a^2}$, and $R = |\mathbf{x} - \mathbf{x}'|$, μ is the shear modulus, and ν is the Poisson's ratio. The parameter a represents the width of the dislocation core, which we call here the non-singular parameter. The residual traction $\tilde{\mathbf{t}}$ based on this expression is non-singular in the neighborhood of the points of intersection of the dislocation lines with the domain boundary. For computational purposes, the line integral in expression (17) is converted into a sum of integrals over linear dislocation elements of finite length; see [20] for further details. For the sake of completeness, we have also developed complimentary expressions for the non-singular elastic rotation and strain tensors; these are given, respectively, by

$$\omega_{ml}^{\mathrm{ns},\infty}(\mathbf{x}) = \frac{1}{16\pi}\oint_L [\epsilon_{lik}(b_i\partial_m + b_m\partial_i) + \epsilon_{imk}(b_l\partial_i + b_i\partial_l)]\partial_j\partial_j R_a\,\mathrm{d}x'_k,$$
$$\varepsilon_{ml}^{\mathrm{ns},\infty}(\mathbf{x}) = -\frac{1}{16\pi}\oint_L b_p\left[\left(\delta_{km}\epsilon_{pql} + \delta_{kl}\epsilon_{pqm} - 2\delta_{lm}\epsilon_{pqk}\right)\partial_q\partial_j\partial_j R_a + \frac{2}{1-\nu}\epsilon_{pjk}\partial_l\partial_j\partial_m R_a\right]\mathrm{d}x'_k. \tag{18}$$

Downloaded By: [Oak Ridge National Laboratory] At: 20:54 4 September 2009

Downloaded By: [Oak Ridge National Laboratory] At: 20:54 4 September 2009

The FEM computational algorithm for the image stress field proceeds as follows:

(i) For a given dislocation configuration in a finite domain, extend all dislocation segments intersecting the surface to infinity. The new configuration consisting of the actual configuration inside Ω and the virtual dislocations is called the *augmented dislocation configuration*.

(ii) Calculate the residual surface traction from the infinite domain stress of the augmented dislocation configuration, reverse its sign and use the result to determine the nodal forces acting at the boundary nodes of the FEM mesh for the image field solution. The residual traction is required only at the quadrature points of surface element.

(iii) Check to see if Equation (3) is satisfied by the computed nodal forces. Here we focus mainly on the sum of the nodal forces $\sum \mathbf{F}_n = \mathbf{F}_R$, which is zero if it captures the traction integral in (3) exactly. Non-zero values of the sum may arise due to a coarse FEM mesh, inadequate quadrature order or boundary traction singularities.

(iv) Subtract the rigid-body motion by fixing six degrees of freedom in the resulting FEM system of equations. Rigid translation is prevented by setting the displacement of a point equal to zero in three directions, and rigid rotation is prevented by setting the displacement of three other points equal to zero, in one (different) direction per point.

(v) Solve the FEM system of equations for the displacement field, obtain the strain from the displacement, and then use the strain to compute the image stress using Hooke's law. The image stress is then added to the infinite-domain solution to fix the overall stress.

The resulting finite element system has the form: $\mathbf{K}\tilde{\mathbf{u}}^h = \mathbf{F}$, where $\mathbf{K}$ is the stiffness matrix, $\tilde{\mathbf{u}}^h$ the displacement vector, and $\mathbf{F}$ the nodal force vector. As noted above, this system cannot be solved without subtracting the rigid-body motion, which is accomplished by fixing six degrees of freedom as explained above. If $\mathbf{F}_R$ (defined in step (iii) above) is sufficiently close to zero, the solution of the FEM system yields boundary reactions that are sufficiently close to the nodal forces computed using the residual traction, which means that the conditions (3) are accurately satisfied. To ensure that this indeed is the case, the mesh resolution and quadrature order are selected to ensure acceptably small values of $\mathbf{F}_R$. The selection of suitable mesh resolution and quadrature order do, of course, depend on the non-singular parameter a.

6. Convergence tests and application

A simple dislocation configuration has been used to test the above computational algorithm for the image field of dislocations. The domain Ω is chosen to be a cube of side ℓ, with the origin at the center. The dislocation configuration consists of three segments contained within the cube. Two of these segments are extended to infinity along their respective directions to form the virtual dislocations outside the box. Table 1 summarizes the coordinates of this five-segment configuration. Segment S1 and S5 are virtual segments, representing the extension of segments S2 and S4, respectively to infinity. This configuration is denoted as C1. In order to study the effect the virtual dislocations on

Table 1. Dislocation configuration used to test the computational algorithm.

Segment	Start point[a]	End point[a]	Orientation (ϕ, θ)[b]
S1	∞	$(-0.25, -0.25\sqrt{3}, -0.5)$	$(\frac{\pi}{4}, \frac{\pi}{3})$
S2	$(-0.25, -0.25\sqrt{3}, -0.5)$	$(0, 0, 0)$	$(\frac{\pi}{4}, \frac{\pi}{3})$
S3	$(0, 0, 0)$	$(0, 0, 0.25)$	$(0, -)$
S4	$(0, 0, 0.25)$	$(0.125\sqrt{3}, 0.125, 0.5)$	$(\frac{\pi}{4}, \frac{\pi}{6})$
S5	$(0.125\sqrt{3}, 0.125, 0.5)$	∞	$(\frac{\pi}{4}, \frac{\pi}{6})$

[a]Coordinates in units of the box size ℓ.
[b]ϕ is the angle between the segment and x_3-coordinate. θ is the angle between the projection of segment onto the x_1x_2-plane and the x_1-coordinate.

Downloaded By: [Oak Ridge National Laboratory] At: 20:54 4 September 2009

the resulting image field, an alternate virtual dislocation configuration is considered; a second configuration C2 is constructed from C1 by extending the virtual segments S1 and S5 to infinity at arbitrary angles. Namely, the pair of angles (ϕ, θ) defining the direction of the virtual segments, see Table 1, are set equal to $(0.32\pi, 0.45\pi)$ for segment S1 and to $(0.16\pi, 0.54\pi)$ for segment S5.

The elastic and crystallographic properties of the domain containing the dislocations here are chosen to correspond to a Mo crystal with a shear modulus of 130 GPa and a Poisson's ratio of 0.31. The primary slip systems of Mo are of the type $\bar{a}/2\ \langle 111\rangle\ \{110\}$, with the magnitude of the Burgers vector $b = 2.725$ Å. These Burgers vectors include $\bar{a}/2[111]$, $\bar{a}/2[11\bar{1}]$, $\bar{a}/2[1\bar{1}1]$, and $\bar{a}/2[1\bar{1}\bar{1}]$, with $\bar{a}$ being the lattice parameter (not to be confused with the non-singular parameter a). The Burgers vectors are denoted here by b1, b2, b3 and b4, respectively. The cubic Mo crystal domain under consideration here has an edge length of $\ell = 17.5 \times 10^3\, b$ ($\approx$4.77 μm), and the test dislocation configurations C1 and C2 have Burgers vectors of the type b1.

The convergence of the computational algorithm outlined earlier has been investigated with respect to three parameters: the non-singular parameter a, the FEM mesh density represented by the parameter N_{E} and the order of quadrature Q used in computing the surface forces from the residual traction. Here, the parameter a is expressed in units of Burgers vector. We note that the classical singular solution of dislocations in an infinite domain (see, for example, [27]) is recovered exactly from the non-singular stress expression (17) in the limit $a \to 0$. Hence, the smaller the value of the parameter a, the closer to the singular expression the non-singular solution becomes. As for the FEM implementation, the crystal domain under consideration has been meshed into cubic trilinear (isoparametric) elements constructed by partitioning the cube edges into N_{E} elements; therefore, the solution domain contains a total of N_{E}^3 finite elements. The surface elements are thus square, two-dimensional elements and a quadrature order Q means that each surface element contains Q^2 Gauss quadrature points. As shown below, the appropriate mesh resolution and quadrature order depend on the value of the parameter a, and the interplay between these three parameters is studied by investigating the quantity $\sum \mathbf{F}_{\mathrm{n}} = \mathbf{F}_{\mathrm{R}}$ as a function of the these parameters. This quantity, which is the integral of the traction over the boundary, is itself the numerical error of the traction integral because it must be zero if the nodal boundary forces are computed accurately.

Figure 2 shows a plot of the boundary traction integral error $\mathbf{F}_{\mathrm{R}}$ for a non-equilibrium situation in which the image traction is due to the interior dislocation segments alone;

Downloaded By: [Oak Ridge National Laboratory] At: 20:54 4 September 2009

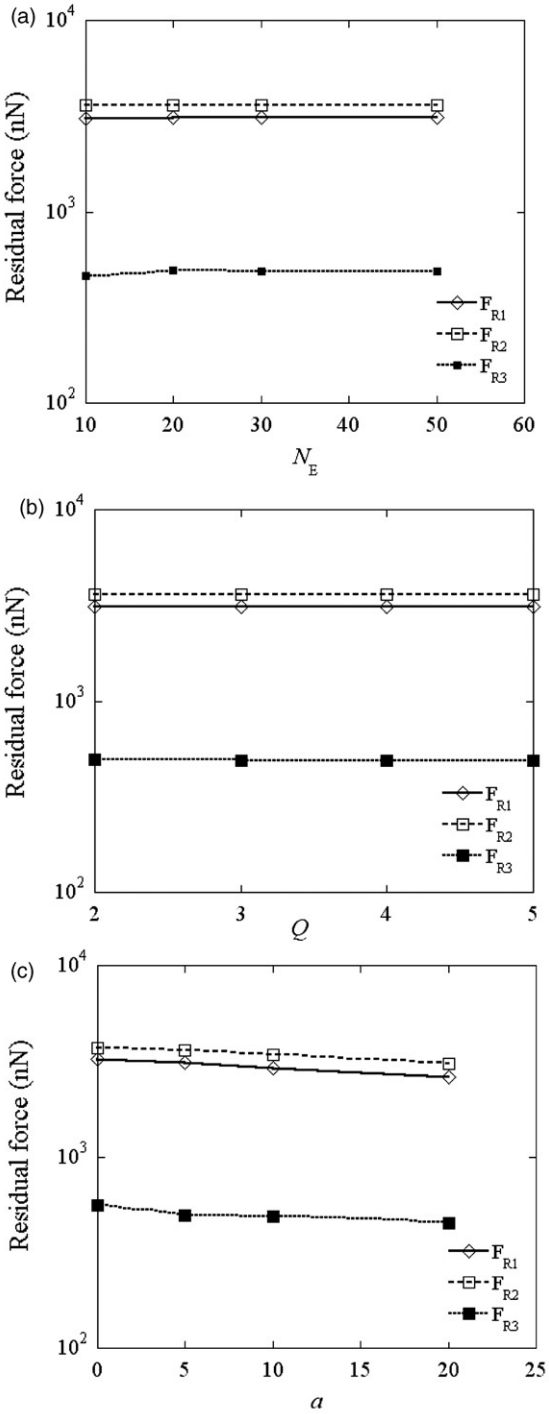

Figure 2. Boundary traction integral error $\mathbf{F}_R$ corresponding to interior segments of dislocation configuration C1. (a) $Q = 3$ and $a = 5$. (b) $N_E = 30$ and $a = 5$. (c) $N_E = 30$ and $Q = 2$.

see Table 1. Figure 2a shows the magnitudes of the components of $\mathbf{F}_R$ as a function of the mesh density parameter N_E for $a = 5$ and $Q = 3$. In Figure 2b, these magnitudes are plotted against Q for $N_E = 30$ and $a = 5$, while in Figure 2c, they are plotted against a for $N_E = 30$ and $Q = 2$. The large imbalance of the residual traction for all values of a, Q and N_E clearly demonstrates the need for virtual segments to ensure equilibrium.

Figure 3 displays $\mathbf{F}_R$ as a function of the FEM mesh density parameter for $Q = 3$ (part a) and as a function of quadrature order for $N_E = 30$ (part b), for the augmented dislocation configuration C2. In both cases, the non-singular parameter a is set equal to zero, meaning that the singular field of dislocations is used to compute the residual traction. We note that, because the analytical form of the residual traction does satisfy equilibrium, the magnitudes of the components of the error $\mathbf{F}_R$ are about an order of magnitude smaller than their counterparts displayed in Figure 2, where the dislocation

Downloaded By: [Oak Ridge National Laboratory] At: 20:54 4 September 2009

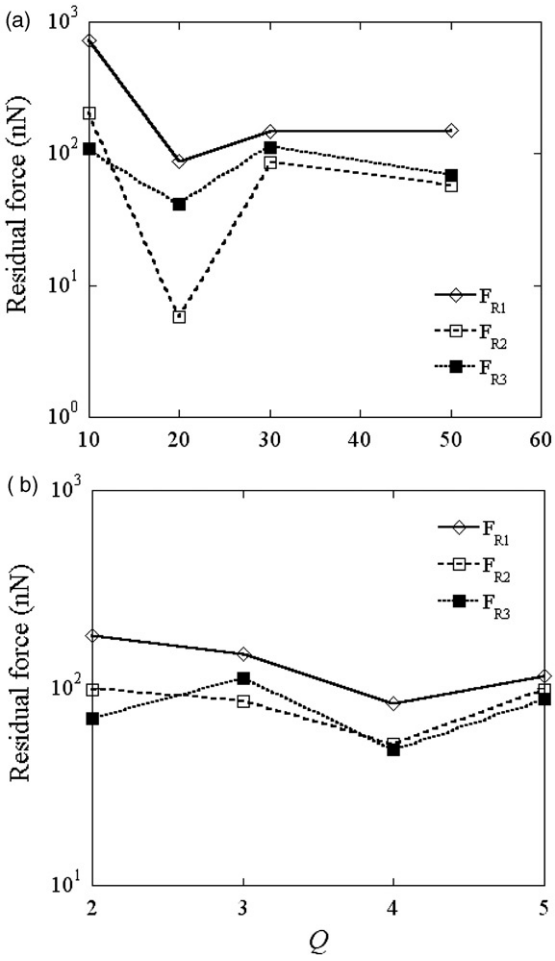

Figure 3. Boundary traction integral error $\mathbf{F}_R$ plotted against mesh density and quadrature order for dislocation configuration C2 when $a = 0$. (a) $Q = 3$. (b) $N_E = 30$.

configuration does not satisfy equilibrium. However, in spite of the fact that the singular stress field of the augmented configuration C2 satisfies equilibrium and reasonably good mesh density and quadrature order were used, the error $\mathbf{F}_R$ is still unacceptably high. This indicates that, for the mesh resolution and quadrature order used, the nodal force values are inaccurate due to the high gradients of the residual traction near the points of intersection of dislocations with the surface. Therefore, a further increase in the mesh resolution and/or quadrature order is required to capture the nodal forces accurately. This result is consistent with the findings in [6], where fine resolution and high quadrature order, up to $Q = 10$, were used in some cases. We remark here that, in dislocation dynamics simulations, the image field is required to be updated at every time step, and thus a finely resolved FEM mesh combined with a high quadrature order can raise the computational cost significantly.

The examples in Figures 2 and 3 show clearly that accurate and practical FEM computations of the image field of dislocations in bounded domains require that both the equilibrium of residual traction and the traction singularities on the boundary be dealt with satisfactorily. This fact is illustrated in the examples shown in Figures 4 and 5. In Figure 4 the magnitudes of the components of $\mathbf{F}_R$ are shown as functions of the mesh density parameter, quadrature order and the non-singular parameter a, for the augmented dislocation configuration C2. In Figure 5 the same is shown for augmented configuration C1. In both cases, the residual traction is based on the non-singular stress formula (17). It is important to note that the components of $\mathbf{F}_R$ decay roughly exponentially to negligible values for moderate mesh density, relatively low quadrature order and small values of the non-singular parameter. Based on Figures 4 and 5, it is obvious that quadrature of fourth or fifth order and a non-singular parameter in the range 5–10 would yield accurate nodal forces at moderate FEM mesh resolution; this corresponds to a/d_q in the range 0.05–0.1, where d_q is the average distance between Gauss quadrature points.

In order to determine the effect of the virtual dislocation construction on the image field, the L_2 norm of the difference between the image stresses corresponding to the augmented configurations C1 and C2 has been computed. In doing so, the following formula has been used:

$$L_2 = \frac{1}{N_E^3}\left[\sum_{k=1}^{N_E^3}\left(\tilde{\sigma}_{ij}^{C1}(k) - \tilde{\sigma}_{ij}^{C2}(k)\right)^2\right]^{1/2}, \quad \text{for } i,j = 1,2,3. \tag{19}$$

The image field was computed here by analytically averaging the stress field over each element and assigning the result to the center of the element. The L_2 norm results are summarized in Table 2. In this particular example, the following parameters were used: $N_E = 30$, $Q = 5$ and $a = 5$. The maximum value of the magnitude of image stress components was on the order of 50 MPa, which occurs at the boundary near the dislocation intersection. The L_2 norm is thus much smaller than the maximum numerical value of the image field in the domain of solution. Although this is a good indicator of the weak effect the virtual dislocation configuration has on the image field, one must take this result with some caution, because it is not just the average difference between the stresses of C1 and C2 that matters. The point-by-point comparison of the fields is also important in assessing the impact of the virtual dislocation construction on the image field. Such a comparison would be difficult to do here because the FEM mesh involves about

Downloaded By: [Oak Ridge National Laboratory] At: 20:54 4 September 2009

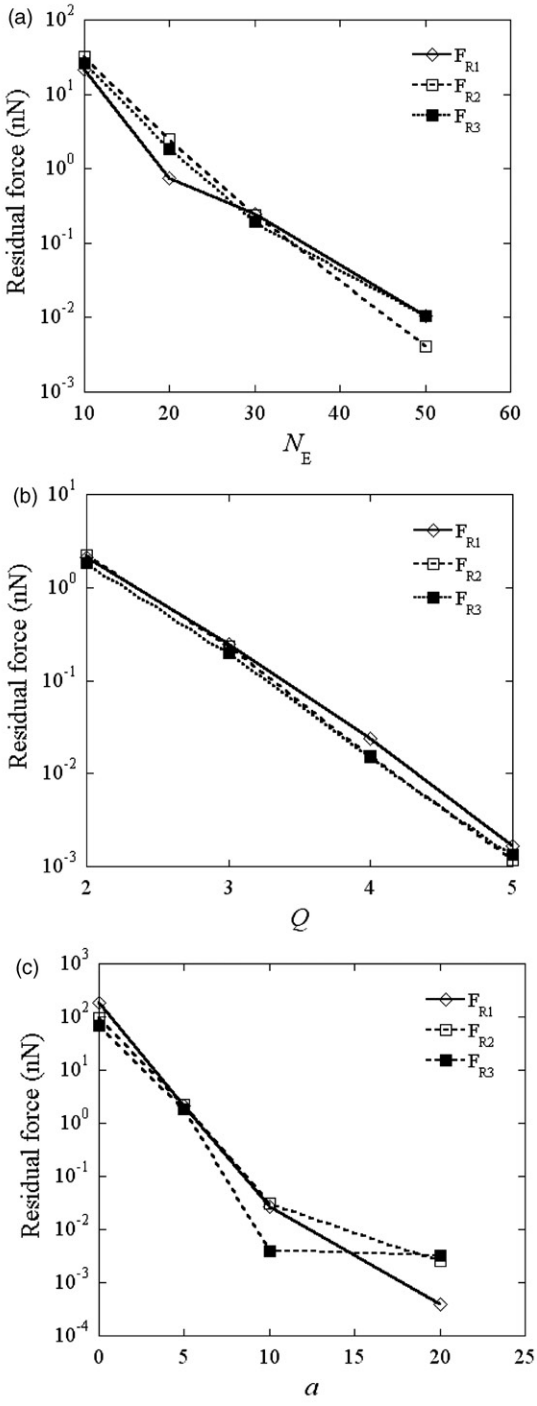

Figure 4. Convergence of the boundary traction integral error with mesh density, quadrature order and non-singular parameter for dislocation configuration C2. (a) $Q=3$ and $a=5$. (b) $N_E=30$ and $a=5$. (c) $N_E=30$ and $Q=2$.

Downloaded By: [Oak Ridge National Laboratory] At: 20:54 4 September 2009

Downloaded By: [Oak Ridge National Laboratory] At: 20:54 4 September 2009

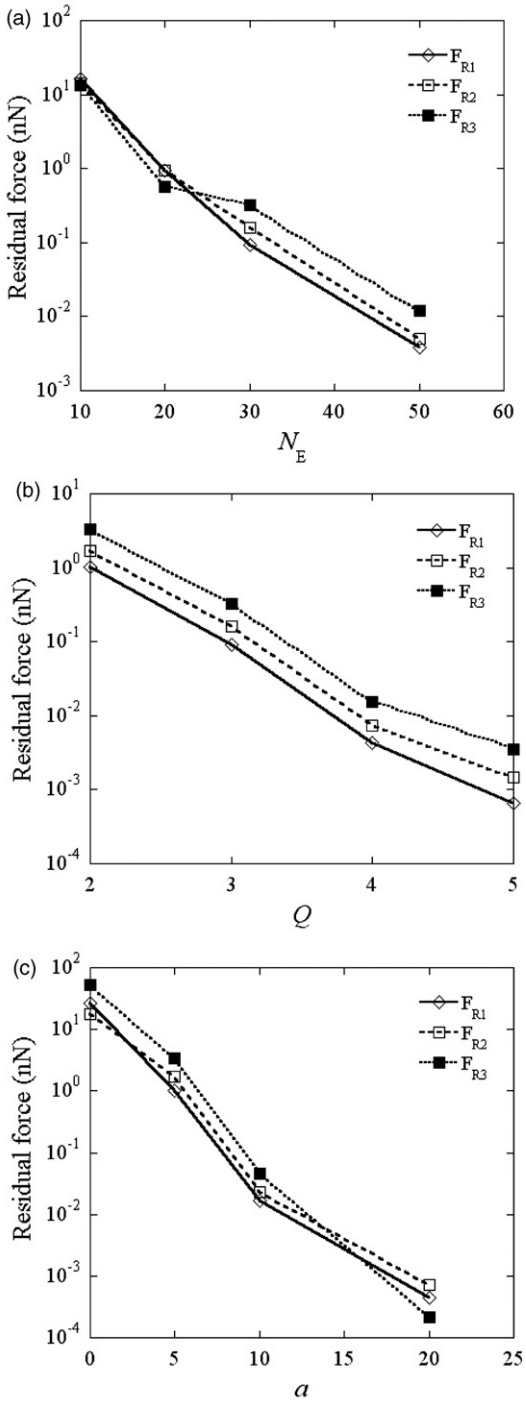

Figure 5. Convergence of the boundary traction integral error with mesh density, quadrature order and non-singular parameter for dislocation configuration C1. (a) $Q=3$ and $a=5$. (b) $N_E=30$ and $a=5$. (c) $N_E=30$ and $Q=2$.

Table 2. L_2 norm of the difference between image stresses for augmented dislocation configurations C1 and C2.

Stress component	$\tilde{\sigma}_{11}$	$\tilde{\sigma}_{12}$	$\tilde{\sigma}_{13}$	$\tilde{\sigma}_{22}$	$\tilde{\sigma}_{23}$	$\tilde{\sigma}_{33}$
L_2 norm[a]	0.200	0.130	0.079	0.180	0.068	0.140

[a]in MPa.

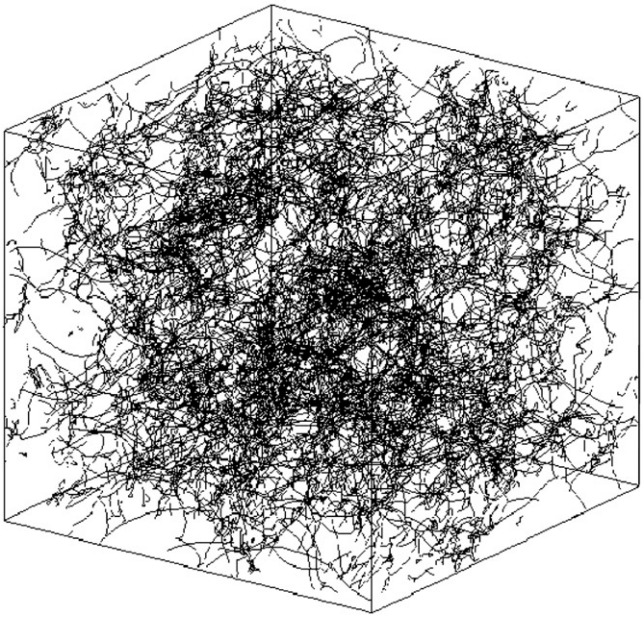

Figure 6. Typical dislocation configuration in Mo crystal of size 4.77 μm strained to 0.5% at strain rate of $10\,s^{-1}$.

Downloaded By: [Oak Ridge National Laboratory] At: 20:54 4 September 2009

27,000 elements. However, we remind the reader that the goal of the current exercise is to test the use of the non-singular infinite-domain solution with the FEM method for image field calculations. Based on Figures 4 and 5, this seems to offer a very good combination of methods to solve for the image field.

For the sake of illustrating the applicability of the solution method outlined here to large scale problems, the method has been used to compute the internal stress arising due to complex dislocation configurations in a cubic crystal volume of size $\ell = 17.5 \times 10^3\, b$. These dislocation configurations have been obtained using the dislocation dynamics simulation code ParaDis [3]; see [28] for the material parameters. We alert the reader here that the method under testing in this section was not used as part of the ParaDiS code simulations. In obtaining the dislocation configurations, the crystal was loaded in the [100] crystallographic direction at a constant strain rate. Because of the multiple slip nature of this loading, the dislocation configuration includes dislocations with the four types of Burgers vectors mentioned previously. A typical dislocation configuration is shown in Figure 6, featuring a large number of dislocation segments. In computing the total stress

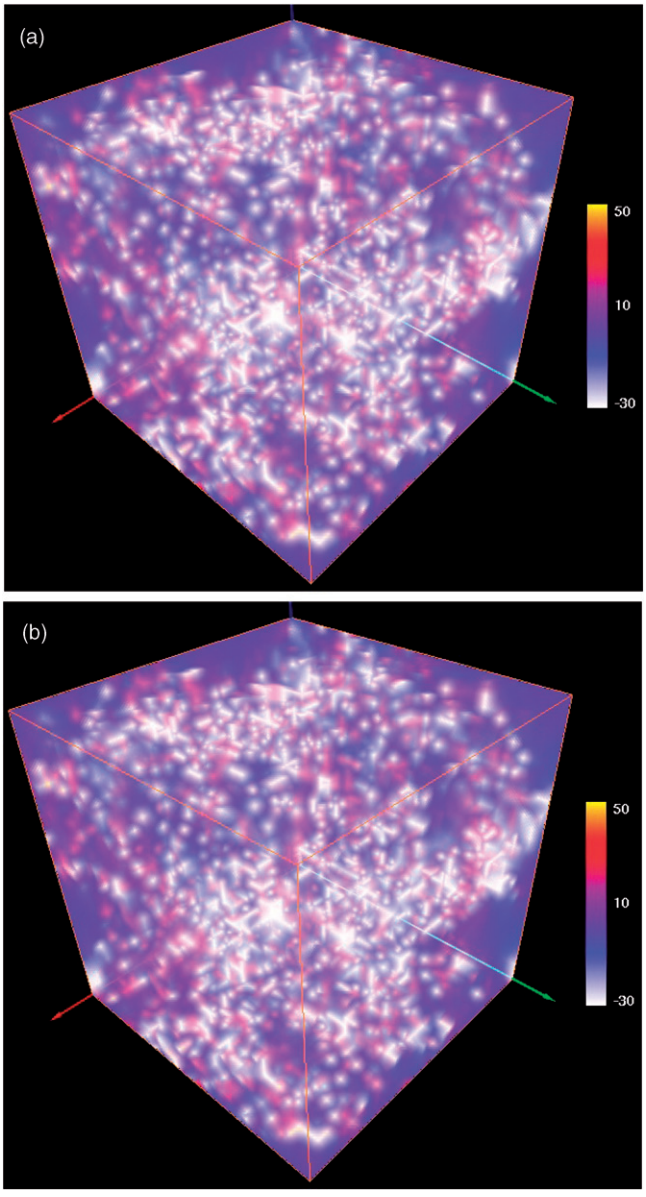

Figure 7. Distribution of σ_{33} in a Mo crystal of size 4.77 μm at strains $\epsilon = 1.5 \times 10^{-2}$ (in a) and $\epsilon = 2.23 \times 10^{-2}$ (in b) and strain rate $\dot{\epsilon} = 1\,\mathrm{s}^{-1}$.

field, the non-singular parameter a is set to 5, and the image field is computed using a mesh parameter $N_E = 30$ and quadrature order $Q = 5$; both the infinite-domain and image field contributions were averaged analytically over each finite element and this value (in units of MPa) was assigned to the center of the element to display the result.

A sample calculation of the internal stress field in the crystal is shown in Figure 7. The figure displays the spatial distribution of the stress component σ_{33} at crystal strain

Downloaded By: [Oak Ridge National Laboratory] At: 20:54 4 September 2009

$\epsilon = 1.5 \times 10^{-2}$ (part a) and $\epsilon = 2.23 \times 10^{-2}$ (part b), where the crystal was strained at a rate $\dot{\epsilon} = 1\,\mathrm{s}^{-1}$. The complexity of the internal stress distribution is apparent in this sample result, and it is obvious that a formal statistical analysis method is required in order to make quantitative statements about such distributions. While a full analysis of the stress distribution is outside the scope of this paper, some qualitative remarks on its salient features are in order. One important feature is that the stress distribution can exhibit a tendency toward internal patterning (Figure 7). The stress distribution is of course connected with the spatial distribution of the dislocation density. Hence, the discreteness of the dislocation density is the decisive factor in dictating the spatial fluctuations of the internal stress. Other results (not shown here) indicate that the morphological features of stress patterning depend strongly on the level of crystal strain and strain rate, which is not surprising since these two parameters are known to affect dislocation density and its distribution in the crystal.

The internal stress field of dislocations in crystals must of course average to zero over the crystal volume because dislocations are internal stress sources. The local value of the internal stress thus represents the local stress fluctuation relative to its volume average. These fluctuations can be characterized quantitatively by the spatial correlation of the internal stress distribution. Accordingly, statistical analyses along these lines are underway with the goal of establishing a direct link between dislocation dynamics simulations and sub-micrometer resolution 3D X-ray microscopy measurements of the internal elastic fields (strain and rotation) in crystals containing high densities of dislocations [21,22,29,30]. Establishing such a link will be critical for detailed evaluation of the predictive capabilities of mesoscale plasticity models.

Downloaded By: [Oak Ridge National Laboratory] At: 20:54 4 September 2009

7. Concluding remarks

The present paper contains two contributions. The first contribution is a formalism for the elastic boundary value problem of dislocations in bounded crystals that rigorously describes stress equilibrium, and the second is the demonstration of an approximate solution of this problem based on the concept of virtual dislocations.

With respect to the elastic boundary value problem addressed in Section 3, it is important to emphasize that the formalism presented here provides a definitive method for describing stress equilibrium in bounded crystal domains with complex dislocation configurations, irrespective of how the boundary value problem is solved. This result provides a useful framework for solving the long-range interaction problem in dislocation dynamics problems when considered along with the conclusion reached earlier by one of the authors in [7], that the bounded crystal and RVE are equivalent when it comes to image stress calculation.

The greatest benefit of this framework is expected to be for the case of an RVE, where no assumptions (such as periodicity) regarding the dislocation configuration outside of the simulated crystal volume are needed to compute the evolution of dislocation structure inside the domain. This is a remarkable result given the complexity and cost of computing the image fields when periodic boundary conditions are considered in the case of RVE simulation.

The approximate solution presented in Sections 5 and 6 has been pursued here mainly to examine the use of FEM techniques in conjunction with non-singular infinite-domain

dislocation stress [20] for solving the image field problem of dislocations. We have shown that the removal of the singularity from the classical solution of the stress field of dislocations makes it significantly easier to use the FEM technique to solve the image field boundary value problem. In particular, it has been shown that residual dislocation boundary traction can be captured accurately into nodal forces when the singularity of the dislocation stress field is smeared over a distance of several Burgers vectors. This, in turn, makes it possible to solve the image field problem for complex dislocation configurations by the FEM method using only moderate quadrature order and moderate finite element mesh resolution. The importance of this result is that it opens the door for the use of the non-singular stress solution developed in [20] in conjunction with the FEM technique to solve image field boundary problems within dislocation dynamics models.

The complex nature of the internal elastic fields in crystals containing high densities of dislocations underscores the need for statistical analysis to obtain quantitative measures of the spatial distributions of these fields. Combined with statistical models of the dislocation populations, e.g. those developed in [28], such analysis of internal elastic fields will help close the crystal mechanics part of the kinetic theory of dislocations [31] self-consistently. In addition, statistical analyses of the internal elastic fields of dislocations will make possible a quantitative comparison between the predictions of dislocation dynamics simulations and 3D X-ray microscopy measurements of internal elastic fields in deformed crystals [21,22,29,30].

Downloaded By: [Oak Ridge National Laboratory] At: 20:54 4 September 2009

Acknowledgements

AE and JD were supported in part by UT-Battelle LLC subcontract # 4000058790 at Florida State University. BL was supported by the Department of Energy, Office of Science, Division of Materials Sciences and Engineering. AE wishes to thank the ParaDiS code team of Lawrence Livermore National Laboratory for making the code available for use during the course of this study.

References

[1] B. Devincre and L. Kubin, Phil. Trans. Math. Phys. Eng. Sci. 355 (1997) p.2003.
[2] N.M. Ghoniem, S.H. Tong and L.Z. Sun, Phys. Rev. B 61 (2000) p.913.
[3] A. Arsenlis, W. Cai, M. Tang et al., Model. Simul. Mater. Sci. Eng. 15 (2007) p.553.
[4] H.M. Zbib, T.D. de la Rubia, M. Rhee et al., J. Nuclear Mater. 276 (2000) p.154.
[5] E. van der Giessen and A. Needleman, Model. Simul. Mater. Sci. Eng. 3 (1995) p.689.
[6] D. Weygand, L.H. Friedman, E. van der Giessen et al., Model. Simul. Mater. Sci. Eng. 10 (2002) p.437.
[7] A. El-Azab, Model. Simul. Mater. Sci. Eng. 8 (2000) p.37.
[8] A. El-Azab, in *MRS Symposium Proceedings*, Volume 538, T. Diaz de la Rubia, T. Kaxiras, V. Bulatov et al. eds., Material Research Society, Warrendale, PA, 1999, p.107.
[9] M. Tang, W. Cai, G. Xu et al., Model. Simul. Mater. Sci. Eng. 14 (2006) p.1139.
[10] E.H. Yoffe, Phil. Mag. A 6 (1961) p.1147.
[11] B.J. Shaibani and P.M. Hazzledine, Phil. Mag. A 44 (1981) p.657.
[12] Jaafar A. El-Awady, S. Bulent Biner and N.M. Ghoniem, J. Mech. Phys. Solid. 56 (2008) p.2019.
[13] T.A. Khraishi, H.M. Zbib and T.D. de la Rubia, Mater. Sci. Eng. A 309–310 (2001) p.283.
[14] C.R. Weinberger and W. Cai, J. Mech. Phys. Solid. 55 (2007) p.2027.
[15] C. Lemarchand, B. Devincre and L.P. Kubin, J. Mech. Phys. Solid. 49 (2001) p.1969.

[16] C. Lemarchand, B. Devincre, L.P. Kubin et al., in *MRS Symposium Proceedings*, Volume 538, T. Diaz de la Rubia, T. Kaxiras, V. Bulatov et al. eds., Material Research Society, Warrendale, PA, 1999, p.63.
[17] T. Mura, *Micromechanics of Defects in Solids*, Kluwer Academic, Netherlands, 1993.
[18] K.W. Schwarz, J. Appl. Phys. 85 (1999) p.108.
[19] N. Kinoshita and T. Mura, SIAM J. Appl. Math. 44 (1984) p.524.
[20] W. Cai, A. Arsenlis, C.R. Weinberger et al., J. Mech. Phys. Solid. 54 (2006) p.561.
[21] B.c. Larson, A. El-Azab, W. Yang et al., Phil. Mag. 87 (2007) p.1327.
[22] B.C. Larson, J.Z. Tischler, A. El-Azab et al., ASME J. Eng. Mater. Tech. 130 (2008) pp.021024:1–10.
[23] R. de Wit, J. Res. National Bureau of Standards – A. Phys. Chem. 77 (1973) p.49.
[24] T. Mura, *Boundary problems for dislocation*, in *Dislocations in Solids*, H. Suzuki, T. Ninomiya, K. Sumino and S. Takeuchi eds., University of Tokyo Press, Tokyo, 1985, p.17.
[25] V. Bulatov, M. Rhee and W. Cai, in *MRS Symposium Proceedings*, Volume 653, L. Kubin, J. Bassani, K. Cho et al. eds., Material Research Society, Warrendale, PA, 2001, p.Z1.3.1.
[26] W. Cai, V. Bulatov, J. Chang et al., Phil. Mag. 83 (2003) p.539.
[27] J.P. Hirth and J. Lothe, *Theory of Dislocations*, John Wiley, New York, 1982.
[28] A. El-Azab, J. Deng and M. Tang, Phil. Mag. 87 (2007) p.1201.
[29] B.C. Larson, W. Yang, G.E. Ice et al., Nature 415 (2002) p.887.
[30] W. Yang, B.C. Larson, J.Z. Tischler et al., Micron 35 (2004) p.431.
[31] A. El-Azab, Phys. Rev. B 61 (2000) p.11956.

Downloaded By: [Oak Ridge National Laboratory] At: 20:54 4 September 2009